Low-energy positron diffraction from the (110) surfaces of GaAs and InP

X. M. Chen and K. F. Canter
The Martin Fisher School of Physics, Brandeis University, Waltham, Massachusetts 02254

C. B. Duke and A. Paton
Xerox Webster Research Center, 800 Phillips Road, Webster, New York 14580

D. L. Lessor
Pacific Northwest Laboratory, K5-17 ISB-1, Richland, Washington 99352

W. K. Ford*
Advanced Materials Center and Department of Physics, Montana State University, Bozeman, Montana 59717
(Received 17 December 1992)

The intensities of 16 nonequivalent beams of normally incident positrons diffracted from the (110) surfaces of GaAs and InP are reported. The sample temperature was approximately 110 K. The intensities were measured over the energy range 30 eV $\leq E \leq$ 200 eV. The atomic geometries of GaAs(110) and InP(110) were extracted from these intensities via their comparison with the predictions of a multiple-scattering model using the criterion of minimization of the x-ray R factor. The best-fit surface geometries resulting from these analyses are approximately bond-length-conserving top-layer and second-layer rotations characterized by the tilt angles ($\omega_1 = 28.5° \pm 2.5°$, $\omega_2 = -3.5° \pm 3°$) for GaAs(110) and ($\omega_1 = 24.5° \pm 1.5°$, $\omega_2 = -3.0° \pm 3°$) for InP(110). Comparable low-energy electron intensity data were obtained and analyzed for InP(110) leading to ($\omega_1 = 31^{\circ}{}^{+3^{\circ}}_{-5^{\circ}}$ and $\omega_2 = -3° \pm 3°$). Small changes ($\Delta d \leq 0.07$ Å) in the bond lengths associated with the top-layer species are characteristic of the best-fit structures, but of these, only a small contraction ($\Delta d/d \leq 3\%$) of the bond between the top-layer cation and second-layer anion seems likely to lie outside the uncertainties inherent in the analysis.

I. INTRODUCTION

In many areas of physical and chemical technology, such as crystal growth, catalysis, corrosion, hardening and passivation treatments, heterojunction formation, thin-film barriers and superlattices, the properties of the crystal surface exert a dominant influence.[1] The most basic information required to understand the surface characteristics of materials is a detailed description of the geometrical arrangement of atoms in a surface or adsorbed layer.[2,3] Of the many surface-sensitive techniques, low-energy electron diffraction (LEED) is one of the most often used.[2-9] LEED theory gives a sufficiently accurate description of the multiple scattering of electrons incident on solid surfaces to be used to determine surface atomic geometries for both metals[7] and semiconductors[8,9] via comparison of calculated and measured I-V profiles (diffracted beam intensities as functions of incident electron energy). Numerous structures have been determined in this fashion.[4-9] A commonly used measure of the difference between experimental and calculated I-V profiles is the x-ray R factor (R_x).[10] Generally, the smaller the R_x, the better the theoretical model describes the diffraction process and, thus, the more reliable the determination of the surface structure. Surface structures are usually obtained by minimizing R_x or comparable measures of the goodness of the fit between calculated and experimental I-V profiles.[5-10]

Recent structure determinations of semiconductor surfaces by low-energy positron diffraction (LEPD) have raised the possibility that LEPD not only constitutes a surface structure determination methodology comparable to LEED, but that it may also add to the precision of the specification of a surface structure which has been determined by LEED alone.[11-14]. LEPD studies of CdSe(10-10),[11-13] CdSe(11-20),[11-13] and GaAs(110),[14] have demonstrated significantly improved agreement between calculated and experimental I-V profiles relative to corresponding LEED studies. Although this result could imply an improved level of precision in a structure determination using LEPD, such speculation would be premature without a thorough investigation of the factors responsible for the improved agreement between the calculated and experimental LEPD I-V profiles as well as the sensitivity of this agreement to the relevant structural parameters of the surface being studied. The purpose of this work is to explore the nature of surface structure determination via LEPD and to extend our prior analysis of GaAs(110) to InP(110). The (110) surface structures of all III-V and II-VI semiconductors show remarkable similarities to one another.[9,15] Of these, the GaAs(110) surface is noteworthy among semiconductor surfaces for the accuracy and confidence with which its surface atomic geometry is known. The surface structure of GaAs(110) determined by LEPD agrees well with the structure determined by LEED and several other techniques.[14]

0163-1829/93/48(4)/2400(12)/$06.00

In this paper we report the results of a detailed LEPD investigation of GaAs(110) and InP(110) and compare them with the results of analogous LEED studies. In Secs. II and III we describe how the experimental and theoretical I-V profiles, respectively, are obtained. In Sec. IV we indicate the procedure used to analyze these I-V profiles to determine the atomic geometries of the surface. The differences between LEPD and LEED determinations of the GaAs(110) and InP(110) surfaces are examined in Sec. V with an emphasis on the role played by the nature of the probe-particle-target–ion-core interaction on the sensitivity and accuracy of LEPD versus LEED. We conclude in Sec. VI with an indication of the important results which have emanated from our analysis.

II. EXPERIMENTAL PROCEDURE

A. Apparatus and sample preparation

The apparatus for our LEPD measurements is described in detail elsewhere.[11–13] Briefly, β^+ decay positrons are emitted from a 100-mCi Na-22 source placed behind a W(100) thin-film moderator which is 1 μm thick. Approximately 2×10^{-4} of the positrons thermalize in the moderator, diffuse to the other side of the film, and escape as monoenergetic $\sim$3 eV positrons. These positrons then undergo two stages of moderation in order to enhance the beam brightness.[16] A final beam flux of 10^4 e^+/s is focused on the sample surface with a convergence angle less than 1° and beam diameter of 0.5–1.0 mm over the energy range 20–250 eV. Elastically diffracted positrons from the sample surface passed through a hemispherical retarding field analyzer (RFA) and are detected by a two-dimensional (2D) positron sensitive detector. The position of any detected positron is digitized to address a memory location in a 2D buffer. The counts in the selected memory address are then increased by 1, yielding a 2D histogram that comprises the diffraction pattern. Computer control was used to set the incident beam energy, focus the beam onto the sample surface, enable the 2D buffer to accumulate data for a chosen time interval, read the diffraction data from the 2D buffer, and store the data as a file on hard disk. The LEPD energy range converged was 30 to 200 eV. For this energy range, the beam diameter on the sample averaged 0.75 mm and the beam motion was less than 0.5 mm.

Quantitative LEED measurements were also performed on InP(110) using the LEPD diffractometer by reversal of relevant polarities. In order to produce an electron beam with the same axis of incidence as used for LEPD, the last positron remoderation cathode aperture was flooded with electrons emitted from a filament located behind the aperture. This resulted in a beam with poorer emittance (approximately a factor of 4 times larger) than we obtained with the remoderated positron beam.

The GaAs crystals were Si doped with a concentration of 10^{18} cm^{-3}. The InP crystals were Zn doped with a concentration of 4×10^{18} cm^{-3}. The samples were rectangular bars of dimension of $5\times5\times25$ mm with the (110) surface parallel to the 5×5 mm surface. Grooves 0.5-mm deep were cut at 1.5-mm intervals on one of the rectangular faces before being mounted on the sample holder. The samples were mounted in a copper holder with a high thermal and electrical conductivity silver epoxy (microcircuit silver) and baked at 10^{-2} torr for more than 10 h at 200 °C to both degas and set the epoxy. The samples were then introduced into our sample chamber on a manipular sample mount which was coupled to a liquid-nitrogen reservoir via a copper braid. Cooling of the samples to 110 K was accomplished by pumping dry nitrogen through a heat exchanger in liquid nitrogen and into the reservoir. The (110) surface is the natural cleavage plan of GaAs and InP. The samples were cleaved along the grooves in a vacuum at 6×10^{-11} torr to produced clean (110) surfaces. Within minutes after cleaving, portions of the surface which gave a sharp 1×1 LEED pattern were located with respect to the sample boundaries using a display LEED system. Surface areas as large as 2×4 mm giving sharp 1×1 LEED patterns were typical. The normal incidence condition was determined from the symmetry of the diffraction patterns ($-hk$ beam equivalent to the hk beam) obtained. We estimate that this determination of normal incidence was accurate to within 1°. The sample was then rotated so as to face the incident positron beam. The boundaries of the sample relative to the beam were obtained by observing inelastically scattered positrons as the sample was translated past the beam. Once the coordinates of the boundaries were determined, the sample could be positioned with the incident positron beam being incident on the good portions of the sample. The quality of the LEPD patterns versus sample position also were examined to verify our sample positioning procedure.

Each cleaved surface was used for a maximum of two weeks. The cleanliness of the surface at room temperature was checked by comparing the room-temperature diffraction data from a freshly cleaved surface to that from a surface two week after cleaving. Specifically, I-V profiles were obtained by measuring the intensity of a given diffracted beam as a function of the energy of the incident positrons. No difference was observed between the two data sets within 1%. This lack of contamination of the InP(110) and GaAs(110) surfaces at room temperature is especially impressive in view of the fact that small ($\approx$10%) degradations in the overall intensity, but not in the shape, of the I-V profiles were observed when the samples were held at 110 K for 24 h. This was to be expected since the sticking coefficients are very small at room temperature [10^{-8} for the O_2 to GaAs(110) surface, for example] and gases physisorbed at low temperature readily desorb at room temperature.[17] The low-temperature diffraction data were taken as a series of separate runs; each run took a maximum of 20 h and covered a selected energy range. After each run, the sample was warmed to room temperature in 3 h in order to degas the physisorbed molecules. The energy ranges for different runs overlapped each other. Each run was separated into 5 to 8 repeated scans over the same energy range to minimize the influence of possible beam instabilities and surface contamination at low temperature. Each scan took about 2 to 3 h.

B. Data acquisition

The positron beam intensity as a function of incident energy was measured just before each run using an electrostatic parallel-plate mirror mounted on a sample manipulator. By swinging the mirror to face the positron beam, the mirrored flux relative to the diffracted flux could be determined accurately without any assumptions about the detector efficiency. The sample cooling process took approximately 90 min to reach 110 K. This was followed immediately by a maximum run of 20 h. Following a run, the beam intensity as a function of energy was again measured to check beam stability. The beam instability was less than 3%. The influence of the surface contamination was checked by comparing the first scan I-V profiles to the last scan I-V profiles. The I-V profiles from the last scan (20 h later) were about 10% weaker than that from the first scan. The uniformity of the 2D position sensitive detector and the accuracy of the normal incident angle was verified by comparing the I-V profiles of the equivalent beams. All the equivalent beams had the same experimental I-V profiles within statistical errors.

C. Data reduction

The raw data recorded by the 2D imaging system comprised hundreds of digitized diffraction patterns at different incident energies. Each pattern exhibited 10 to 30 diffraction spots. The task of the raw data analysis was to get the intensity of each spot above background and the corresponding statistical error. Figure 1 shows a typical 7-scan cumulative LEPD spot pattern. We defined two concentric inner and outer boxes. The inner box was large enough to enclose each diffraction spot. The counts in the region between the inner box and the outer box were assumed to be background counts due to dark noise and small amounts of positronium formed by inelastically backscattered positrons. A suppressor voltage of 5 V below the incident energy was sufficient to reduce any background due to inelastically scattered positrons to insignificant levels. The average number of background counts per pixel was scaled to obtain the background in the inner box. The spot intensity was obtained by subtracting the corresponding background from the total counts in the inner box. This background subtraction procedure was checked periodically by moving the analysis boxes to regions of the 2D histogram where there were no diffraction spots and verifying that the analysis yielded zero intensity, within statistical errors, associated with the central box. For a given energy of the incident positron beam, the spot intensity and the corresponding statistical error were then converted to absolute diffracted beam intensities by dividing the recorded counts (minus background), per unit time, by the positron beam intensity versus incident energy measured just before the run. The absolute spot intensities as functions of the beam energy comprised the experimental I-V profiles from which surface atomic geometries were obtained via comparison with calculated profiles.

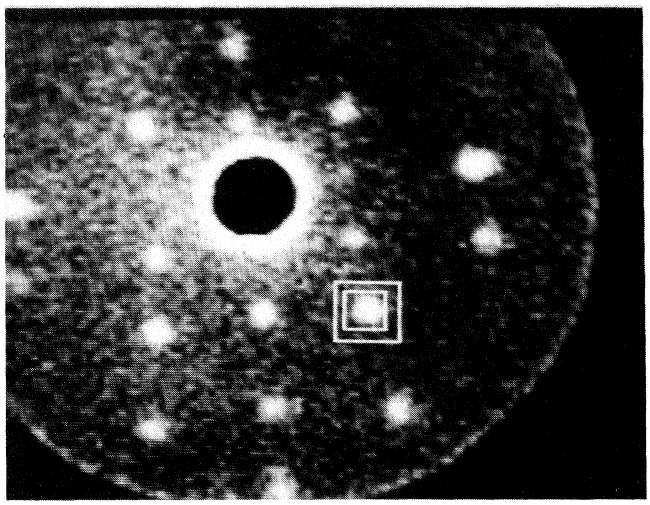

FIG. 1. Digital LEPD spot pattern from GaAs(110). The boxes indicate the region of the detector used to obtain the spot intensity (inner box) and background intensity (outer box) to be subtracted in order to obtain the coherently diffracted intensity in the I-V profiles.

The data files, i.e., the histogrammed diffraction spot patterns for the energy values covered in a run, were analyzed separately for each run. The averaging of the symmetry equivalent beams also was performed separately for each run. The runs were comprised of overlapping as well as duplicate energy scans and were checked for repeatability of the intensities over the entire composite energy range of 30–200 eV covered in the experiment. In addition to checking the repeatability of the intensities with respect to the incident energy, we also took the data on a second cleaved surface and found that the resulting data agreed with the first cleaved data within statistical uncertainties. The χ-squared per degree of freedom for any one taken against the statistically weighed average of all the other runs, when adjusted by a normalization constant, was always found to be statistically consistent with unity. The normalization constants for the runs varied among themselves from unity with a root-mean-square deviation of only 4%. By making this small normalization correction to each run we were able to eliminate, to within statistical uncertainty, any errors due to small drifts in the intensity due to changes in the sample surface contamination and/or incident-beam intensity drifts. We feel that the errors associated with data reproducibility in the final cumulative experimental I-V measurements, which are to be compared with the model calculations, are reliably represented by the Poisson statistical errors, i.e., the square root of the total recorded counts for each beam, including detector background.

III. MODEL CALCULATIONS

The LEPD and LEED I-V data were analyzed using the multiple-scattering model of Duke and Laramore,[18,19] which is a generalization of an analysis of Beeby[20] to include thermal vibrations of the ion cores and complex values of the electron or positron self-energies. Charge particle scattering by crystal ion cores is described by

energy-dependent phase shifts which are calculated from the potential distribution experienced by the scattering particle. This potential is approximated by a muffin-tin form calculated from the potential and charge distributions of isolated atoms, which are obtained from a relativistic self-consistent Hartree-Fock-Slater calculation.[21] A $\rho^{1/3}$ exchange term is used in calculating the isolated atom potentials. To obtain the crystal potentials, suitable potentials for the scattering of electrons or positrons from isolated atoms are superimposed with bulk crystal coordination. The muffin-tin radius is taken to be the crossover point of the atomic potentials between two nearest-neighbor atoms. The resulting muffin-tin potential, measured relative to that at the crossover point, is inserted into a radial Schrödinger equation, which is integrated to give the scattered wave phase shifts. The inner potential V_0 between the muffin tins, measured from the vacuum, is taken to be an adjustable parameter in the fitting procedure. For electrons, an energy-dependent Hara exchange is used in the phase-shift calculation, as is appropriate for electrons more than 10 eV above the Fermi level of the electron gas.[22] The major difference in the scattering potential seen by positrons and by electrons is in the sign of the electrostatic term, the absence or presence of exchange being secondary.[23] The positron phase shifts for scattering from In and P are shown in Figs. 2(a) and 2(b), respectively. The phase shifts for electrons are shown in Figs. 3(a) and 3(b) and are essentially identical to those reported by Ford *et al.*[24] Positron phase shifts for In and P are similar, while electron phase shifts for In and P are very different—a result which will be important in the interpretation of our results. All the calculations reported here were performed using six phase shifts. Seven phase shifts were used for testing convergence.

In the multiple-scattering calculations, the semi-infinite crystal is replaced by a slab of 12 bilayers (12 layers each of In and P). A complete multiple-scattering calculation is done on the outer eight bilayers, with contributions from the next four bilayers to the scattering amplitudes computed individually and added to the scattering amplitudes from the eight outer bilayers. Two attenuation models were used for the LEPD structural analysis: the constant V_i model, where V_i is the imaginary part of the self-energy, and the Oliva model.[25] The Seah-Dench attenuation model[26] was used for LEED calculations. The computer program used to perform the calculations was an adaptation of that described by Meyer *et al.*[27]

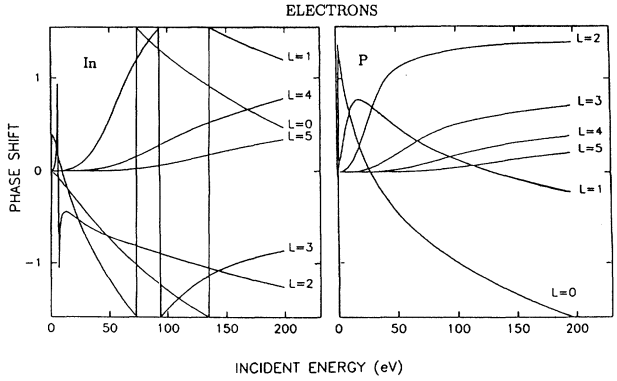

FIG. 2. Electron scattering phase shifts in radians for In (left panel) and P (right panel).

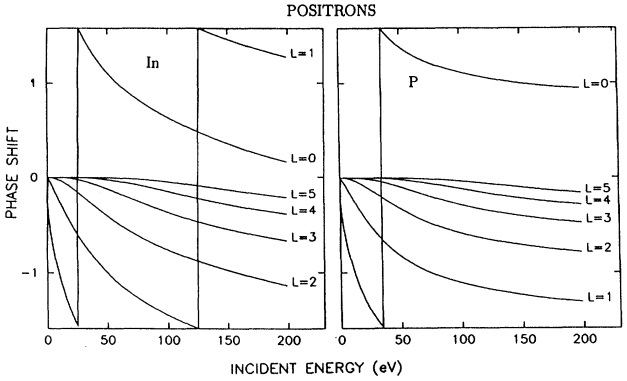

FIG. 3. Positron scattering phase shifts in radians for In (left panel) and P (right panel).

Five independent structural parameters were determined via a comparison of the calculated and measured *I-V* profiles. A schematic diagram of the structural features of the zinc-blende (110) surfaces is shown in Fig. 4. Since a zinc-blende (110) surface has reflection symmetry, relaxation of the surface will not change the x coordinates of any atom. Thus, two independent variables are needed to specify the position of each atom. Four independent variables are needed to specify the position of the two atoms in a unit cell on the surface. We choose

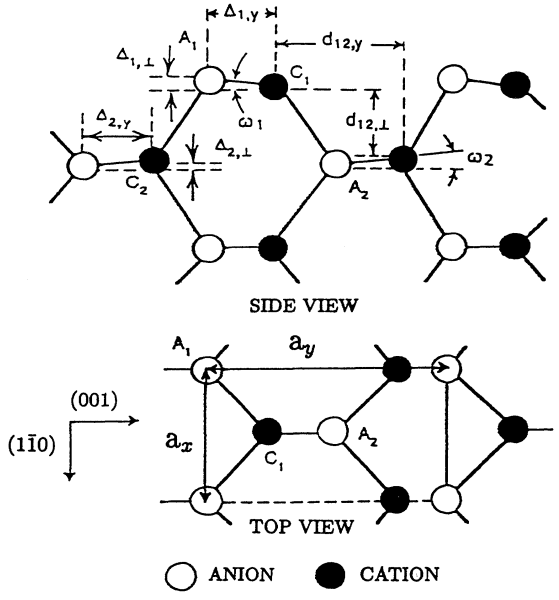

FIG. 4. Schematic indication of the atomic geometry and independent structural parameters for the zinc-blende (110) surface. The first- and second-layer shear angles are given as $\omega_i = \arctan(\Delta_{i,\perp}/\Delta_{i,y})$ for $i=1,2$. A negative ω_1 and a positive ω_2 are depicted in the drawing. The anion (cation) in the ith layer is designated by $A_i(C_i)$.

them to be the perpendicular components $\Delta_{1\perp}$ of shear in the first bilayer, and the three bond lengths C_2-A_1, C_1-A_1, and C_1-A_2, where C_i-A_j indicates the distance between the cation in bilayer i and the neighbor anion in bilayer j. The relaxation of the second bilayer is assumed to be a bond-length-conserving rotation. Thus, the bond lengths are not adjustable and only one structural parameter needs to be varied. For this purpose, we chose $\Delta_{2\perp}$, i.e., the shear in the second bilayer. All other structure parameters, such as the bond rotation angles ω_1 and ω_2 in the top and second bilayers, respectively, may be calculated from these five parameters. Relaxations in the third and deeper bilayers are neglected. Several nonstructural parameters, which are related to the inner potential models,[14] are also obtained from the fit of the measured intensities to the calculated ones.

IV. STRUCTURE ANALYSIS

We take the x-ray R factor R_x (Ref. 10) as a measure of the goodness of fit between the experiment and calculated I-V profiles. Traditionally, each beam is normalized independently when calculating this R factor. We also use another procedure which we call the global R factor, R_{XG}, in which all the beams were normalized by a single "global" constant. Since the calculated I-V profiles are determined by the guessed surface structural and nonstructural parameters, the R factor is also a function of these parameters. The simplex search method[28] was used to determine the minimum in the appropriate R factor. The parameters which minimize the R factor are referred to as the "best-fit" structural and nonstructural parameters of the surface studied. In addition to V_0, two parameters corresponding to the Oliva model, for LEPD, and three to the Seah-Dench model for LEED, were scanned in the simplex searches. For LEPD, a single-parameter attenuation model, i.e., constant V_i, also was employed in the simplex searches.[29]

In the present study, 16 nonequivalent beams set were used to define the set of measured I-V profiles to be described by the calculated intensities. They are 01, 0-1, 02, 0-2, 03, 0-3, 13=−13, 1-3=−1-3, 12 =−12, 1-2 =−1-2, 11=−11, 1-1, −1-1, 10=−10, 21=−21, 20=−20, 2-1=−2-1. For this data set, simplex searches were initiated and allowed to continue until the spread in each of the five structural parameters among the simplex vertices was smaller than 0.005 Å. When these conditions are satisfied, the spread in R factor is less than 0.0005.

As a check that the automated simplex searches did not accidentally converge on suboptimal local minima in the R factor versus structural and nonstructural parameter space, we also computed the R factor as a function of one of the parameters, while holding the other parameters fixed at their original best-fit values. Several such "R-factor scans" are discussed below. This procedure was carried out for several parameters in the model; not only as a check on the simplex searches, but equally important, as a means of assessing the sensitivity of the agreement between calculated and experimental I-V profiles to important features of the surface structure.

Extensive studies were carried out using different energy ranges and different attenuation models as well as the two different R factors, R_x and R_{XG}. The results determined from LEPD are listed in Table I for GaAs(110) and in Table II for InP(110). The first row of entries for Tables I and II are the parameters resulting from R_{XG} minimization simplex searches. All other entries correspond to results from R_x minimization simplex searches. The tables show the results of several different structural parameter determinations corresponding to different energy regions of analysis, attenuation models, as well as R_x and R_{XG} optimizations. The principal purpose of carrying out a variety of structural determinations was to estimate the magnitude of systematic errors in the structural determination due to the use of varying empirical models of the imaginary part of the optical potential and of varying samples of the intensity data. The good agreement between the structural determination using the Oliva model,[25] which describes positron scattering in a free electron gas, and the constant V_i model,[29] suggests that the LEPD structural determinations are relatively insensitive to the precise manner in which the attenuation of the incident beam is treated. Of the various results presented in Tables I and II, we regard the first row entries as our preferred structural determinations. The errors which we assign to the structural parameters will be discussed in Sec. V.

Figures 5 and 6 demonstrate that the top-layer rotation angles ω_1 determined by the simplex searches for GaAs(110) and InP(110), respectively, correspond to a true minimum in R factors, as opposed to a false location minimum.[30] They also demonstrate the sensitivity of the R factors to ω_1. For each of the surfaces, the locations of the minimum in the traditional R_x and the global R_{XG}

TABLE I. GaAs(110) surface structures determined by LEPD using different attenuation models, different R factors, and different energy ranges. In the top row the structure resulted from a simplex minimization of R_{XG}. In the second row it resulted from minimizing R_x. The nomenclature C_i-A_j indicates the bond length between the cation in layer i and the anion in layer j. The structural variables are defined in Fig. 4.

Energy	Model	C_2-A_1 (Å)	C_1-A_1 (Å)	C_1-A_2 (Å)	$\Delta_{1\perp}$ (Å)	$\Delta_{2\perp}$ (Å)	ω_1	ω_2	V_0 (eV)	R_x	R_{XG}
30–180	V_i=5.2 eV	2.435	2.438	2.439	0.666	−0.087	28.5°	−3.5°	0.53	0.0925	0.0954
30–180	V_i=5.0 eV	2.442	2.430	2.406	0.652	−0.081	28.2°	−3.3°	0.53	0.0822	0.0992
30–180	Oliva	2.431	2.435	2.394	0.652	−0.082	28.2°	−3.1°	0.96	0.0789	
50–131	Oliva	2.438	2.460	2.372	0.639	−0.091	2.68°	−3.6°	1.3	0.0685	
40–181	Oliva	2.429	2.447	2.380	0.654	−0.096	27.6°	−4.0°	1.28	0.0808	
60–180	Oliva	2.438	2.423	2.396	0.654	−0.091	28.6°	−3.8°	1.12	0.104	

TABLE II. InP(110) surface structures determined by LEPD using different attenuation models, different R factors, and different energy ranges. In the top row the structure resulted from a simplex minimization of R_{XG}. In the second row it resulted from minimizing R_x. The nomenclature C_i-A_j indicates the bond length between the cation in layer i and the anion in layer j. The structural variables are defined in Fig. 4.

Energy	Model	C_2-A_1 (Å)	C_1-A_1 (Å)	C_1-A_2 (Å)	$\Delta_{1\perp}$ (Å)	$\Delta_{2\perp}$ (Å)	ω_1	ω_2	V_0 (eV)	R_x	R_{XG}
30–180	V_i=4.7 eV	2.521	2.540	2.476	0.605	−0.077	24.3°	−3.0°	1.38	0.0924	0.1530
30–180	V_i=4.7 eV	2.529	2.521	2.467	0.623	−0.085	25.7°	−3.3°	2.30	0.0831	0.1673
30–180	Oliva	2.525	2.524	2.473	0.620	−0.091	25.6°	−3.6°	2.00	0.0831	
50–131	Oliva	2.525	2.534	2.483	0.624	−0.099	25.4°	−3.9°	0.53	0.0667	

scans versus ω_1 are in good agreement. The R factor versus ω_1 scans for the constant V_i model and the Oliva model exhibit essentially no difference. The global R factor, though larger than the traditional R_x factor due to the use of fewer adjustable normalization constants, exhibits a sharper minimum. This is consistent with the observation of a sharper minimum in R_{XG} than in R_x for CdSe LEPD studies.[13] Since the intensities of all the diffraction beams were measured simultaneously, there should be no necessity to use different normalization constants for different beams.

The sensitivity of R_{XG} to the second-layer rotation angle is shown in Figs. 7 and 8 for GaAs(110) LEPD and InP(110) LEPD, respectively. All other parameters were held fixed at the values obtained from the simplex search minimization of R_{XG}, i.e., the values listed in the first row of Tables I and II. For reasons discussed in the following section, we also wanted to investigate the differences between the sensitivity of LEPD and LEED to parallel displacements for InP(110). For this purpose we have chosen to consider the traditional R factor R_x. The sensitivity of R_{XG} to $\Delta_{1,y}$ for InP(110) is shown in Fig. 9.

As an additional check that the surface conditions of our InP(110) cleaved samples were indeed the same as those for other investigators' LEED studies, i.e., well ordered and contaminant free below the few atomic percent level, we obtained LEED data on our samples for the purpose of comparison. The R_x and R_{XG} versus ω_1 scans from our InP(110) LEED measurements obtained from the same surface used for the LEPD measurements are shown in Fig. 10. In the case of LEED, the relative intensities of the various beams are usually incorporated in the structure analysis by use of the integrated beam R factor R_I.[30] In Fig. 10 we also include an R_{XG} versus ω_1 scan. Both R-factor scans shown correspond to the same structural parameters obtained from an R_x minimization simplex search over the energy range 40–181 eV, using the Seah-Dench attenuation model.[26] The structural parameters determined this way are given in Table III. Also given in Table III are the results of the most modern LEED structural determination of InP(110), carried out by Ford *et al.*,[24] which are representative of several earlier LEED studies. Extending the energy range of analysis to 30–181 eV produced a negligible change in the best-fit structure parameters. The agreement between our LEED results and those of Ford *et al.* is very good, particularly in view of the poor emittance of our LEED beam.

In addition to the quantitative measure of agreement between experimental and calculated I-V profiles that can

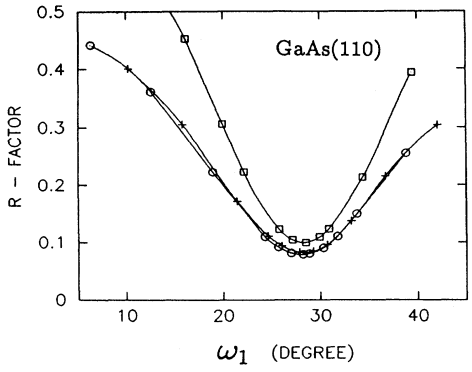

FIG. 5. R factor as a function of ω_1 for LEPD from GaAs(110). All structural and nonstructural parameters were initially determined by the simplex search procedure. Then all parameters except ω_1 were kept fixed when we calculated the R factor as a function of ω_1. □ denotes ω_1 for global R_{XG}, + denotes the ω_1 scan for the traditional R_x using the constant V_i model, and ○ denotes the ω_1 scan for the traditional R_x using the Oliva model.

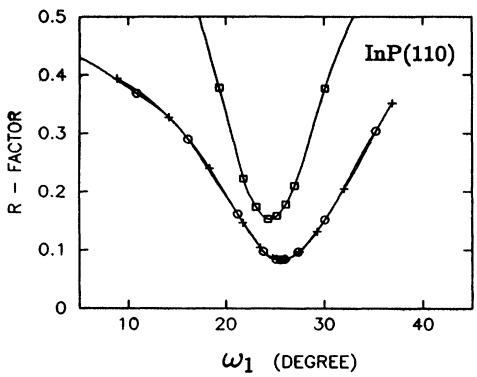

FIG. 6. R factor as a function of ω_1 for LEPD and InP(110). All structural and nonstructural parameters were initially determined by the simplex search procedure. Then all parameters except ω_1 were kept fixed when we calculated the R factor as a function of ω_1. □ denotes the ω_1 scan for global R_{XG}; + denotes the ω_1 scan for the traditional R_x using the constant V_i model; and ○ denotes the ω_1 scan for the traditional R_x using the Oliva model.

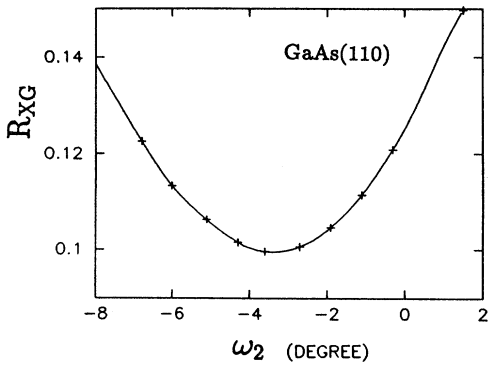

FIG. 7. Global R_{XG} as a function of ω_2 for LEPD from GaAs(110). All other structural and nonstructural parameters were initially determined by the simplex search procedure and were kept fixed.

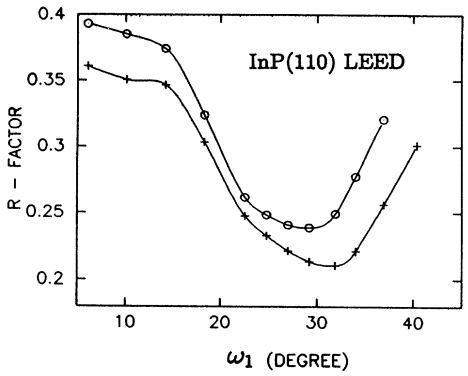

FIG. 10. R factor as a function of ω_1 for LEED from InP(110). All structural and nonstructural parameters were initially determined by simplex search procedure, then all parameters except ω_1 were kept fixed when we calculated the R factor as a function of ω_1. ○ denotes the ω_1 san for global R_{XG} and the Seah-Dench model and + denotes the ω_1 scan for the traditional R_x and the Seah-Dench model.

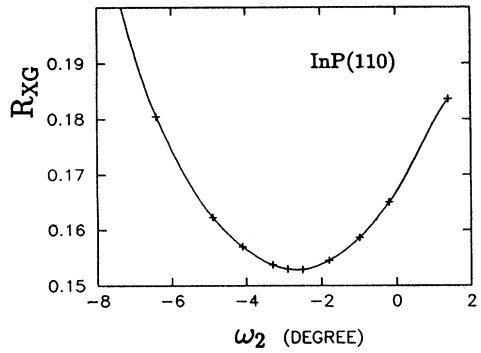

FIG. 8. Global R_{XG} as a function of ω_2 for LEPD from InP(110). All other structural and nonstructural parameters were initially determined by the simplex search procedure and were kept fixed.

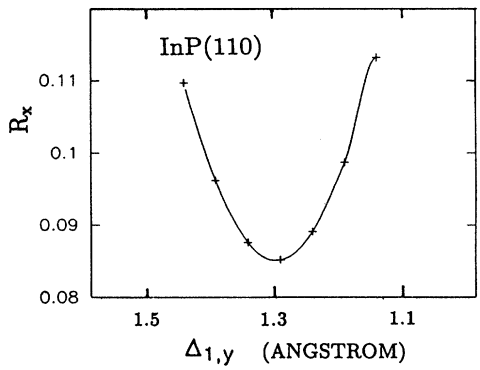

FIG. 9. R_x as a function of $\Delta_{1,y}$ for LEPD from InP(110). All other structural and nonstructural parameters were initially determined by the simplex search procedure and were kept fixed.

be provided by R factors, visual comparisons between LEPD experimental and the best-fit calculated I-V profiles for GaAs(110) and InP(110) are also relevant and are offered in Figs. 11 and 12, respectively. The calculated profiles correspond to the structural parameters obtained from the R_{XG} minimization simplex searches. Accordingly, the calculated profiles shown have not been individually normalized to each experimental diffracted beam profiles. A single global normalization constant as applied to the calculated profiles so as to make the total integrated intensity of the calculated and experimental beams the same. Because of the poorer emittance of our LEED beam, and hence larger diffraction spot sizes, our LEED data are of slightly lower quality than our LEPD data and other investigators' LEED data. The best agreement between calculated and experimental LEED studies to date of InP(110), and to our knowledge any other compound semiconductor to date, was obtained in the recent LEED studies of Ford *et al.*[24] which yielded an R_x equal to 0.16 as compared with our value of 0.21.

V. COMPARISON OF LEED AND LEPD

The results presented in the previous section raise two issues. First, why are the R factors associated with the best fits to the LEPD data so much smaller than those for the LEED data, and, moreover, what is the significance of this fact? Second, since the LEED and LEPD analyses do not, in general, yield identical surface atomic geometries, what is the intrinsic accuracy of each of the two analyses and how are differences between the diffraction process in LEED and LEPD reflected in the structural parameters which they predict? In this section we discuss each of these two issues, in turn.

It is helpful in discussing both issues to identify the types of uncertainties which can arise when comparing measured and calculated LEED or LEPD intensities.[5,6]

TABLE III. InP(110) surface structures determined by LEED. The nomenclature C_i-A_j indicates the bond length between the cation in layer i and the anion in layer j. The structural variables are defined in Fig. 4.

Measurement	C_2-A_1 (Å)	C_1-A_1 (Å)	C_1-A_2 (Å)	$\Delta_{1\perp}$ (Å)	$\Delta_{2\perp}$ (Å)	ω_1	ω_2	V_0 (eV)	R_x
This work	2.54	2.52	2.53	0.752	−0.055	32.0°	−2.0°	10.9	0.21
Ford *et al.* (Ref. 24)	2.55	2.52	2.49			31.1°	−0.53°	8.5	0.16

The first is errors in the data. These can arise from variations in surface composition or morphology which are undetected by surface characterization measurements, from deviations in the beam intensity or the angles of incidence and exit from their nominal values, or from the different characteristics of different measuring instruments (e.g., the Brandeis versus the Princeton versus the Montana State diffractometers). Such sources of data error occur in addition to the statistical errors associated with the finite numbers of counts encountered in our digital detector apparatus as discussed in Sec. II C.

The second source of uncertainty is associated with the use of a finite sample of intensities. Thus, structures obtained by using different subsets of the total intensity data base give rise to different estimates of the surface structure parameters, as evident from Tables I and II. The range of data used in our analysis greatly overdetermines the surface atomic geometry from the perspective of statistical estimation theory, as has been exploited to propose simplified automated structure analysis methodologies for more complex adsorption systems.[31] Neverthe-

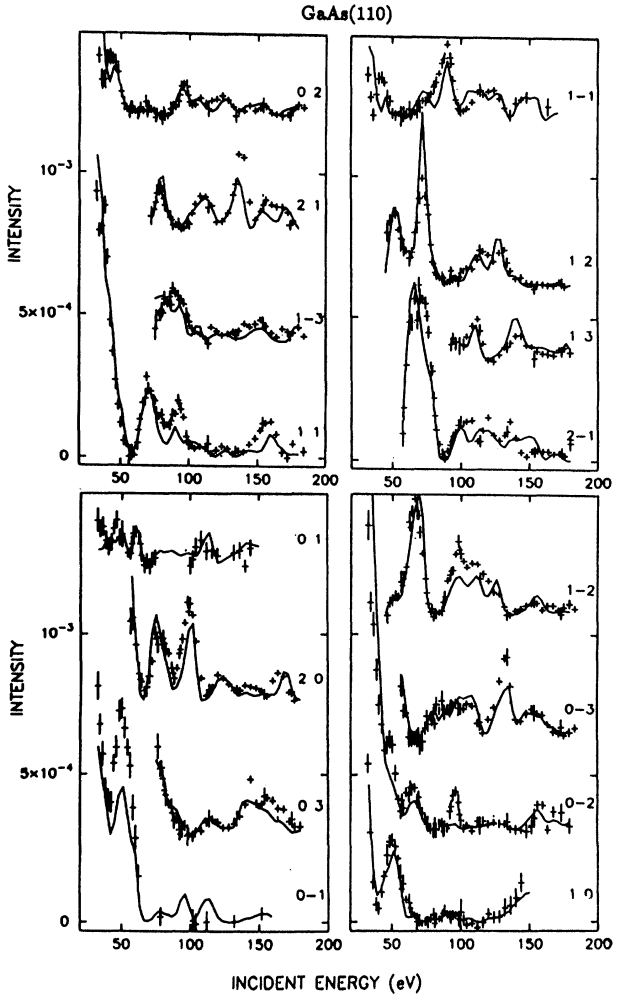

FIG. 11. LEPD experiment I-V profiles for GaAs(110) compared with the best-fit calculated I-V profiles. A global normalization constant was used for all the beam in the comparison. The constant V_i model and R_{XG} were used in the simplex search. Experimental data were taken at 100 K. The individual beam profiles have been displaced vertically for the purpose of clarity. The lowest point for each profile is statistically consistent with zero intensity. The absolute intensity scales shown give the range of excursion from zero intensity for each beam.

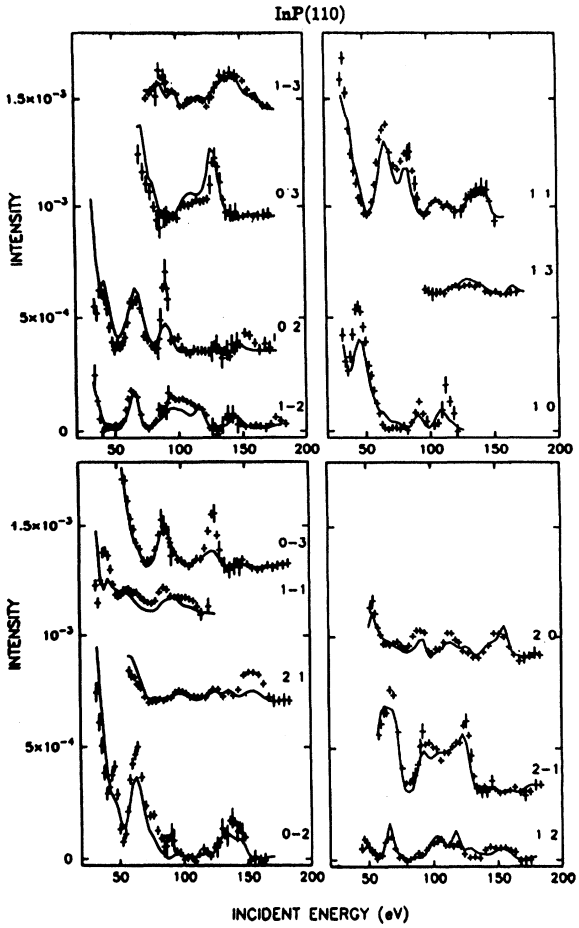

FIG. 12. LEPD experiment I-V profiles for InP(110) compared with the best-fit calculated I-V profiles using a global normalization constant as described in the caption to Fig. 11.

less, the use of different samples from any given set of measured intensities yields different estimates of the structural parameters and hence leads to uncertainties in these estimates.

The third source of uncertainty is the model of the electron-solid or positron-solid interaction. The model used in the present analysis is the multiple scattering of the incident particles from an array of vibrating ion cores described by self-consistent atomic charge densities within muffin-tin radii, embedded in a dissipative electron fluid described by a local complex energy-dependent inner potential. This model can be challenged on either fundamental (e.g., surface loss process are not explicitly included in the model: a big effect at large angles of incidence[32]) or practical (e.g., which model of the inner potential is preferable) grounds. Nevertheless, it has proven remarkably successful in describing LEED and LEPD from a wide variety of materials.[5–9,33] As increasingly precise surface structural features (e.g., surface bond-length changes) are sought from measured intensities; however, its shortcomings may become more significant. Independently, it exhibits features which cause LEED and LEPD to exhibit differing sensitivities to specific aspects of surface structures, and hence to exhibit differing uncertainties in the best-fit structures resulting from R-factor minimization procedures.

As indicated in Sec. II C, we regard systematic errors in the measured I-V profiles to be comparable to or less than the experimental statistical errors. We calculate the contribution of the statistical errors to R_x to be 0.01 for both the LEPD GaAs(11) and InP(110) measurements. Thus, 0.01 would be the minimum value of R_x that could be expected in the limit of "perfect" agreement between the calculated and experimental I-V profiles. Although our LEPD values, $R_x = 0.08$ for GaAs(110) and InP(110), do not meet this criterion for perfect agreement, the visual agreement between the calculated and experimental profiles, as shown in Figs. 11 and 12, is quite good. The principal source of disagreement between the experimental and calculated profiles results from discrepancies in the intensities, but not the locations, of a few isolated peaks. With the exception of these peaks, the calculated and experimental profiles generally agree to within statistical errors.

LEED studies which are directly comparable to our LEPD analyses have been reported recently for the (110) surfaces of both GaAs (Refs. 14 and 34) and InP.[24] Comparison of Fig. 7 in Ford *et al.*[34] with Fig. 11, and of Fig. 5 in Ford *et al.*[24] with Fig. 12, reveals comparable agreement for most beams between the predicted and measured intensities for LEPD and LEED. In the case of LEED, however, large discrepancies occur for a few individual beams [e.g., the (22) beam for both GaAs and InP, the (21) beam for GaAs, and the (1-2) beam for InP]. These greatly reduce the quality of the overall agreement as measured by the R-factor figure of merit and partly account for the poorer R factor for LEED relative to LEPD despite comparable visible descriptions of most beams in the two cases. Moreover, the LEED intensities are large to much higher energies ($E_{\max} \simeq 300$ eV) than the LEPD intensities ($E_{\max} \simeq 150$ eV), leading to further amplification in the magnitude of R_x for those beams for which the fit is less good: an effect which also occurs for LEPD as indicated, e.g., by comparison of the bottom four rows of Table I.

We infer from these observations that the low values of $R_x \approx 0.08$ obtained in the LEPD structure relative to the values of $0.16 \leq R_x \leq 0.18$ obtained in the comparable LEED analyses[14,24] reflect that fact that for the model of the electron-positron-solid interaction described above, dynamical LEED theory produces more accurate calculated I-V profiles when applied to positrons than to electrons. The reason(s) for this situation have not yet been unequivocally established, but it seems likely that the repulsive Coulomb potential experienced by the positrons when scattering from the ion cores is the most important factor.[14,23,33]

We next address the question of the accuracy of the LEPD determined structural parameters for GaAs(110) and InP(110). The essence of the issue which confronts us may be stated simply. We have measured and analyzed LEPD intensities in a fashion which is step-by-step identical to that used for the LEED intensities from GaAs(110) and InP(110) in Refs. 34 and 24, respectively. For InP(110) we further remeasured the LEED intensities and repeated the analysis reported in Ref. 24. For GaAs(110) we repeated[14] the analysis of the data reported in Ref. 34. Yet the surface atomic geometries obtained by LEPD and LEED are not identical as may be seen by comparing the results given in Tables I and II to the comparable LEED analyses in Refs. 14, 24, and 34 (see also Table III). For GaAs(110) the differences lie comfortably within traditional error estimates.[9,24,34] For InP(110), however, they are at best on the borderline of these estimates. A similar result was obtained for the (10-10) and (11-20) surfaces of CdSe.[13] Thus, we must inquire into the origin of these differences and attempt to quantify their significance.

Before describing our error estimates, it is helpful to sharpen the definition of the problem of determining the accuracy of a LEPD or LEED structure analysis. The R-factor methodology which we use to define the "best-fit" structure may be regarded as an extension of Pearson's χ^2 test[35–37] for the probability that the measured intensities fit the energy and angular distribution predicted by the multiple-scattering model. The R_{DE} R-factor introduced by Kleinle, Moritz, and Ertl[31] also may be regarded as a similar extension of the χ^2 test. Thus, the magnitude of R_x or R_{XG} is a measure of the probability that the measured intensities conform to the model predictions. Due to the absence of a theory for the selection of the degrees of freedom variable and of a standard confidence level in the χ^2 test, however, the quantitative values of R factors such as R_{XG} or R_{DE} are of heuristic but not statistical utility.

As discussed earlier, both the measured intensities and the model intensities contain sources of uncertainty ("noise"). Thus, a precise assessment of the accuracy of the LEPD (or LEED) structure analysis requires evaluation of the distribution of measured values of a given structural parameter, given the noise associated with the uncertainties in the data, the model particle-solid interac-

tion, and the other structural parameters. Within a χ^2 test this criterion can be formulated in terms of the range of χ^2 values which can be accepted for proscribed tolerance limits when all of the random variables in the model and measurement vary according to their distributions.[35-37] This range is not well defined, however, without a theory specifying the degrees of freedom associated with the data sampling procedure and whether or not all the other parameters in a given model interaction are allowed to readjust when a given structural parameter is varied. Since this parameter estimation problem is a very general one in data analysis, a body of literature exists on its solution in special cases.[37,38] This theory has not yet been applied systematically to the LEED structure analysis problem, however, so in this paper we limit our consideration to heuristic estimates of the accuracy of the determination of individual structural parameters.[5,31]

An initial estimation of the consequences for R-factor analyses of the various sources of uncertainty described at the beginning of this section was given over a decade ago by Duke *et al.*[39] during the course of a LEED structure analysis for GaP(110). They reported ranges of values of R_x associated with data reproducibility of $(\Delta R_x)_D = 0.1$ (for the LEED data available at that time) and ranges associated with plausible choices of the nonstructural parameters in the model (e.g., the selection of the imaginary part of the inner potential) of $(\Delta R_x)_M = 0.04$. The determination of structures using individual beams as statistically independent samples has been considered in the literature for LEED structure analyses[5] and a number of heuristic studies of the effects of data sampling procedures on the calculation of R factors have been reported.[5,31] A clear description of the variations in R_x associated with the selection of plausible but different samples of intensity data is, however, not available in the literature, to our knowledge.

We have performed global uncertainty estimates for LEPD analogous to those given earlier for LEED from GaP(110). We established in Sec. II C that the uncertainty in R_x associated with data reproducibility is $(\Delta R_x)_D \approx 0.01$. From Tables I and II, we estimate the uncertainties in R_x obtained from the use of varying models of the nonstructural parameters to be $(\Delta R_x)_M \leq 0.02$. From these tables, those associated with the data sampling variations in R_x using the data base shown in Figs. 11 and 12 are estimated to be $(\Delta R_x)_S \leq 0.03$. Thus, the estimated range of R_x values associated with our best fits given in Tables I and II is

$$\Delta R_x = [(\Delta R_x)_{D^2} + (\Delta R_x)_{M^2} + (\Delta R_x)_{S^2}]^{1/2} \simeq 0.04 \ . \qquad (1)$$

This result implies that by virtue of the improvement in data acquisition and sample preparation, as well as the use of the simplex search method to determine nonstructural as well as structural parameters, the range of values of R_x associated with equally plausible "best-fit" analyses for the proscribed data and specified model positron-solid interaction is reduced significantly relative to the earlier LEED study of GaP(110).[39] This fact, plus the reduced values of R_x itself, imply that we clearly can have increased confidence in the structure extracted from the present analysis even though we do not yet have a quantitative statistical measure of the extent of the increase. This conclusion also is valid for the recent LEED studies of GaAs(110) (Refs. 14 and 34) and InP(110).[24]

Turning to the assessment of the uncertainties in specific structural parameters, we need to introduce the additional notion of sensitivity. The variations in R_x generated by the global uncertainty estimates are of varying relevance for estimating the errors on a given structural parameter because they affect to differing degrees the value of that parameter extracted from a given analysis. This is evident from Tables I and II in which the selection of the model of the imaginary part of the inner potential hardly changes the best-fit values of the structural parameters although it generates a range of $\Delta R_x \approx 0.01$. The choice of data to analyze yields proportionally larger changes in the structural parameters associated with $\Delta R_x \leq 0.036$. Evidently the extracted values of the structural parameters are more sensitive to the selection of the data sample than they are to that of the imaginary part of the inner potential.

The sensitivity of R_x and R_{XG} to variations in the major structural parameters, ω_1 and ω_2, is illustrated by Figs. 5 and 7 for GaAs(110) and by Figs. 6 and 8 for InP(110). It is known[30,40] that the shape of the R_x versus ω_1 curves is dominated by the influence of $\Delta_{1,\perp}$ in

$$\omega_1 = \tan^{-1}(\Delta_{1,\perp}/\Delta_{1,y}) \qquad (2)$$

with R_x exhibiting a much smoother behavior as a function of $\Delta_{1,y}$. Figure 9 shows a series of calculations which quantify the variations of R_x with $\Delta_{1,y}$ for LEPD from InP(110). Comparable results for LEED from GaAs(110) and InP(110) may be found in Ref. 9. The sensitivity of R_x to variations in ω_1 for the analysis of our LEED data for InP(110) in estimated by the calculations shown in Fig. 10 (which is directly comparable to Fig. 11 in Ref. 24).

Because of the various sources of uncertainty discussed above, values of the structural parameters extracted from an analysis of a specified sample of intensity data using a given model of the particle-solid interaction are usefully regarded as measurements of random variables each of which exhibits a probability distribution obtained by repeating the analysis many times using equally likely data samples and model interactions.[38] These variables typically would be assumed to exhibit Gaussian distributions about their mean values.[37,38] If we could determine the variances, σ^2 of these distributions, then we could say with 95% confidence that for a measured value p of a given structural parameter that the average value $\langle p \rangle$ of its distribution lies in the range of $p \pm 2\sigma$. In typical analyses of LEED and LEPD intensities,[5-14] the measured values p are extracted from the analysis and estimates of σ, associated with uncertainties in the data and model interaction but not in the selection of the data samples, are sought.

Crude estimates of the confidence limits, i.e., $\pm 2\sigma$ for Gaussian distributions, may be obtained by using calculations such as those given in Tables I and II to assess mea-

sures of the variations in R_x or R_{XG} due to the uncertainty sources of interest and subsequently using Figs. 5–10 to convert these to ranges of uncertainty in the structural parameters. From Tables I and II $\Delta R_x \approx 0.02$ is estimated to be the range associated with statistical uncertainties in the data plus plausible variations in model parameters associated with the simplex best-fit model calculation. Inserting these values into Figs. 5, 6, and 10 gives

$$\omega_1=(\text{LEPD},\text{GaAs},R_x)=28.2°\pm3°\ , \tag{3a}$$

$$\omega_1=(\text{LEPD},\text{InP},R_x)=25.7°\pm2.5°\ , \tag{3b}$$

$$\omega_1=(\text{LEED},\text{InP},R_x)=31.1°{}^{+3°}_{-5°}\ , \tag{3c}$$

using R_x as a figure of merit. Using R_{XG} as the figure of merit but retaining $\Delta R_{XG} \approx 0.02$ as the range of R values given from Figs. 5–8 yields

$$\omega_1=(\text{LEPD},\text{GaAs},R_{XG})=28.5°\pm2.5°\ , \tag{4a}$$

$$\omega_1=(\text{LEPD},\text{InP},R_{XG})=24.3°\pm1.5°\ , \tag{4b}$$

$$\omega_2=(\text{LEPD},\text{GaAs},R_{XG})=-3.5°\pm3°\ , \tag{4c}$$

$$\omega_2=(\text{LEPD},\text{InP},R_{XG})=-3.0°\pm{}^{+3.5°}_{-2.8°}\ . \tag{4d}$$

These estimates treat the structural variables as uncorrelated, whereas they are known to exhibit correlations both among themselves and with non-structural variables (especially V_0). Nevertheless, the process does afford a rough estimate of the confidence limits of the various variables.

The results given in Eqs. (3) and (4) reveal a mild dilemma. The LEPD results for GaAs agree closely with both the LEED results of Ford *et al.*[34] and our own reanalysis of the same data.[14] For InP(110), however, the value of ω_1 obtained from the LEPD analysis is only marginally compatible with that obtained from both our own and other[9,24] analyses of LEED data. The calculations in Table II indicate that this result is not associated with an unusual expansion in the top layer In_1-P_1 bond length. Figure 9 reveals that it cannot be rationalized via a reduced sensitivity of the LEPD analysis to the values of $\Delta_{1,y}$ relative to LEED. Indeed, the converse is the case. Thus, the question arises of whether this is a systematic difference between LEPD and LEED for binary tetrahedrally coordinated compound semiconductors whose anion and cation exhibit significantly different electron scattering factors. The fact that an analogous phenomenon occurs for CdSe (Ref. 13) suggests that fundamental differences between the two techniques might be reflected in this result.

The major difference between LEPD and LEED which is incorporated into our model calculations is the contrast between the anion and cation sublattices. For LEPD, the scattering factors of the two are nearly identical, whereas for LEED they exhibit a large and highly energy-dependent difference as indicated for the total cross sections in Fig. 13. We suspect that distribution functions for the top-layer intersublattice structural variables, i.e., $\Delta_{1,\perp}$ and $\Delta_{1,y}$, are correlated with the difference in the anion and cation scattering factors used in the multiple-scattering calculation of the diffraction process.

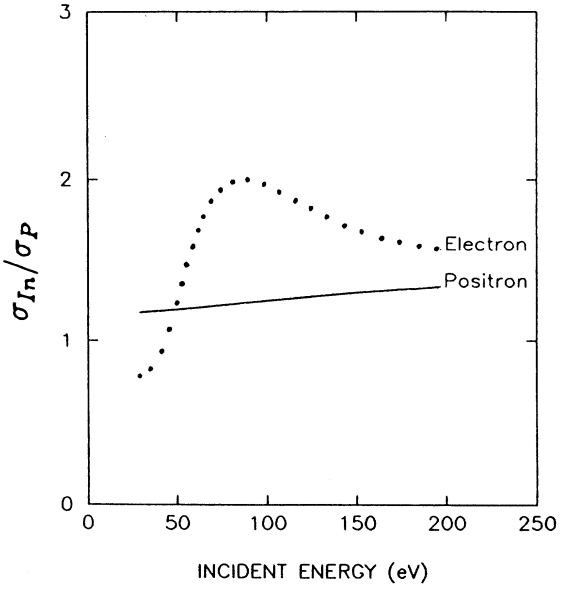

FIG. 13. Ratio of the total cross sections for scattering from In to that for scattering from P for electrons (dotted line) and positrons (solid line) over the energy range of interest for LEED and LEPD.

Specifically, as the scattering factors become more equal, smaller top-layer displacements are required to provide comparable manifestations in the calculated intensities. If true, this conjecture would lead to a more uniform sensitivity of LEPD relative to LEED for top-layer relaxations in binary semiconductors because for LEPD $\sigma_{\text{anion}} \approx \sigma_{\text{cation}}$ for almost all energies and atomic species.[23] Such uniformity, in turn, would lead LEPD to be more accurate than LEED for the study of structural trends among homologous series of binary semiconductor surfaces.[15] Unfortunately, the rudimentary state of statistical error analyses in LEED and LEPD precludes a definite numerical test of this conjecture at the present time.

VI. DISCUSSION

We believe that in the foregoing sections we have established the following results. (1) LEPD is as well suited for (binary) compound semiconductor surface structure analysis as LEED. (2) The quality of the multiple-scattering model fits to the LEPD data consistently exceeds that of the fits to comparable LEED data and leads to equivalent or smaller uncertainties in the structural parameters extracted from these fits. (3) The probable cause of result (2) is the better description of positron-ion-core scattering relative to electron-ion-core scattering afforded by the overlapping atomic charge-density model used to evaluate the ion-core scattering factors. (4) A systematic difference between the values of the structural variables extracted from LEPD and LEED analyses of equivalent data is suggested but not proven, probably associated with the different contrast between the anion and cation sublattices in binary compound semiconductors. If proven, the nearly constant contrast

for positrons across all compound semiconductors would lead to LEPD being the technique of choice to study the systematics of compound semiconductor reconstruction. (5) The extraction of small changes in structural variables (e.g., bond lengths by a few percent, tilt angles by a few degrees) from either LEED and LEPD intensity analyses is greatly hindered by the lack of an adequate statistical theory of the errors in these variables caused by uncertainties in the model of the electron (positron) solid interaction and in the sampling of the intensity data. In particular, uncertainties from the sampling process are rarely considered in the literature and seem to be larger than those associated with either data reproducibility or the model interaction.

It would be attractive to correlate our structural results with recent theories of the systematics of compound semiconductor surface reconstruction.[15,41,42] The small differences between the structures of InP(110) and GaAs(110) plus the difficulty in obtaining precise error estimates reveals, however, that such correlations are premature until a better understanding of items (4) and (5) in the preceding paragraph has been achieved.

ACKNOWLEDGMENTS

Pacific Northwest Laboratory is operated by Battelle Memorial Institute for the Department of Energy under Contract No. DE-AC060-76RLO 1830. Work at Brandeis University was supported by the National Science Foundation (Grant No. DMR-88203450). Computations were supported by the National Center for Supercomputer Applications (Grant No. DMR-910000N). We are indebted to Dr. Steven B. Bolte of the Xerox Webster Research Center for his interest in this work.

*Present address: Intel Corporation, 5200 NE Elam Young Parkway, AL3-15, Hillsboro, OR 97124.

[1]K. H. Rieder, in *Dynamical Phenomena at Surfaces, Interfaces, and Superlattices,* edited by F. Nizzoli, K. H. Rieder, and R. F. Willis (Springer-Verlag, Berlin, 1985), p. 2.

[2]C. B. Duke, Appl. Surf. Sci. **11/12**, 1 (1982).

[3]P. R. Watson, J. Phys. Chem. Ref. Data **6**, 953 (1987).

[4]J. M. Maclaren, J. B. Pendry, P. J. Rous, D. K. Saldin, G. A. Somorjai, M. A. van Hove, and D. D. Vvedensky, *Surface Crystallography Information Service: A Handbook of Surface Structures* (Reidel, Dordrecht, 1987), p. 352.

[5]M. A. van Hove, W. H. Weinberg, and C. M. Chang, in *Low-energy Electron Diffraction: Experiment Theory and Surface Structure Determination,* edited by G. Ertl and R. Gomer, Springer Series in Surface Science Vol. 6 (Springer-Verlag, Berlin, 1986), p. 1.

[6]C. B. Duke, Adv. Chem. Phys. **27**, 1 (1974).

[7]P. M. Marcus and F. Jona, Appl. Surf. Sci. **11/12**, 20 (1982).

[8]A. Kahn, Surf. Sci. Rep. **3**, 193 (1983).

[9]C. B. Duke, in *Surface Properties of Electronic Materials,* edited by D. A. King and D. P. Woodruff (Elsevier, Amsterdam, 1988), pp. 69–118.

[10]R. Zanazzi and F. Jona, Surf. Sci. **62**, 61 (1977).

[11]C. B. Duke, D. L. Lessor, T. N. Horsky, G. Brandes, K. F. Canter, P. H. Lippel, A. P. Mills, Jr., A. Paton, and Y. R. Wang, J. Vac. Sci. Technol. A **7**, 2030 (1989).

[12]T. N. Horsky, G. R. Brandes, K. F. Canter, C. B. Duke, S. F. Horng, A. Kahn, D. L. Lessor, A. P. Mills, Jr., A. Paton, K. Stevens, and K. Stiles, Phys. Rev. Lett. **62**, 1876 (1989).

[13]T. N. Horsky, G. R. Brandes, K. F. Canter, C. B. Duke, A. Paton, A. Kahn, S. F. Horng, K. Stevens, K. Stiles, and A. P. Mills, Jr., Phys. Rev. B **46**, 7011 (1992).

[14]D. L. Lessor, C. B. Duke, X. M. Chen, G. R. Brandes, K. F. Canter, and W. K. Ford, J. Vac. Sci. Technol. A **10**, 2585 (1992).

[15]C. B. Duke, J. Vac. Sci. Technol. A **10**, 2032 (1992).

[16]A. P. Mills, Jr., Appl. Phys. **23**, 189 (1980).

[17]J. M. Seo, Y. Z. Li, S. G. Anderson, D. J. Dow Austuen, U. S. Ayyala, G. H. Kroll, and J. H. Weaver, Phys. Rev. B **42**, 9080 (1990).

[18]C. B. Duke and G. E. Laramore, Phys. Rev. B **2**, 4765 (1970).

[19]G. E. Laramore and C. B. Duke, Phys. Rev. B **5**, 267 (1972).

[20]J. L. Beeby, J. Phys. C **1**, 82 (1968).

[21]W. K. Ford, C. B. Duke, and A. Paton, Surf. Sci. **112**, 195 (1985).

[22]R. J. Meyer, C. B. Duke, and A. Paton, Surf. Sci. **97**, 512 (1980).

[23]C. B. Duke and D. L. Lessor, Surf. Sci. **225**, 81 (1990).

[24]W. K. Ford, T. Guo, K.-J. Wan, and C. B. Duke, Phys. Rev. B **45**, 11 896 (1992).

[25]J. Oliva, Phys. Rev. B **21**, 4909 (1981).

[26]M. P. Seah and W. A. Dench, National Physics Laboratory, Div. of Chemical Standards, NPL Report Chem. No. 82, 1978 (unpublished).

[27]R. J. Meyer, C. B. Duke, A . Paton, A. Kahn, E. So, J. L. Yeh, and P. Mark, Phys. Rev. B **19**, 5194 (1979).

[28]C. W. H. Press, B. P. Flannery, S. A. Tuekolsky, and W. T. Vetterling, *Numerical Methods in C* (Cambridge University Press, Cambridge, 1988).

[29]A. H. Weiss, I. J. Rosenberg, K. F. Canter, C. B. Duke, and A. Paton, Phys. Rev. B **27**, 867 (1983).

[30]C. B. Duke, S. L. Richardson, A. Paton, and A. Kahn, Surf. Sci. Lett. **127**, 135 (1983).

[31]G. Kleinle, W. Moritz, and G. Ertle, Surf. Sci. **238**, 119 (1990).

[32]D. L. Lessor, C. B. Duke, P. H. Lippel, G. R. Brandes, K. F. Canter, and T. N. Horsky, J. Vac. Sci. Technol. A **9**, 1874 (1991).

[33]K. F. Canter, C. B. Duke, and A. P. Mills, in *Chemistry and Physics of Solid Surfaces VII,* edited by R. Vanselow and R. Howe, Springer Series in Surface Science Vol. 22 (Springer-Verlag, Berlin, 1990), p. 183.

[34]W. K. Ford, T. Guo, D. L. Lessor, and C. B. Duke, Phys. Rev. B **42**, 8952 (1990).

[35]K. Pearson, Philos. Mag. **50**, 157 (1900).

[36]R. D. Evans, *The Atomic Nucleus* (McGraw-Hill, New York, 1955), pp. 775–783.

[37]E. R. Dougherty, *Probability and Statistics for the Engineering, Computing, and Physical Sciences* (Prentice Hall, Englewood Cliffs, NJ, 1990), pp. 501–519.

[38]W. Menke, *Geophysical Data Analysis: Discrete Inverse Theory* (Academic, San Diego, 1989), p. 285.

[39]C. B. Duke, A. Paton, W. K. Ford, A. Kahn, and J. Carelli, Phys. Rev. B **24**, 562 (1981).

[40]C. B. Duke and A. Paton, J. Vac. Sci. Technol. B **2**, 237 (1984).

[41]M.-H. Tsai, J. D. Dow, R. P. Wang, and R. V. Kasowski, Phys. Rev. B **40**, 9818 (1989).

[42]J. L. A. Alves, J. Hebenstreit, and M. Scheffler, Phys. Rev. B **44**, 6188 (1991).

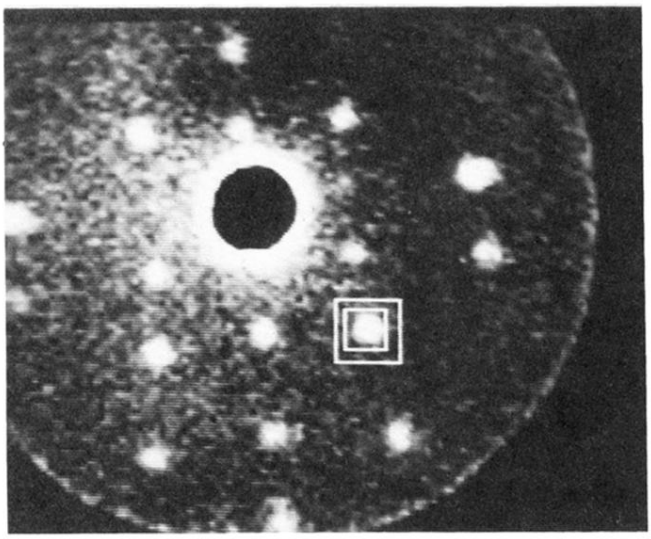

FIG. 1. Digital LEPD spot pattern from GaAs(110). The boxes indicate the region of the detector used to obtain the spot intensity (inner box) and background intensity (outer box) to be subtracted in order to obtain the coherently diffracted intensity in the I-V profiles.